Search for neutral Higgs bosons
of the minimal supersymmetric standard model
in e^+e^- interactions at $\sqrt{s} = 130 - 183$ GeV

L3 Collaboration

M. Acciarri [ab], O. Adriani [q], M. Aguilar-Benitez [aa], S. Ahlen [l], J. Alcaraz [aa],
G. Alemanni [w], J. Allaby [r], A. Aloisio [ad], M.G. Alviggi [ad], G. Ambrosi [t],
H. Anderhub [aw], V.P. Andreev [g,al], T. Angelescu [n], F. Anselmo [j], A. Arefiev [ac],
T. Azemoon [c], T. Aziz [k], P. Bagnaia [ak], L. Baksay [ar], S. Banerjee [k], Sw. Banerjee [k],
K. Banicz [at], A. Barczyk [aw,au], R. Barillère [r], L. Barone [ak], P. Bartalini [w],
A. Baschirotto [ab], M. Basile [j], R. Battiston [ah], A. Bay [w], F. Becattini [q], U. Becker [p],
F. Behner [aw], J. Berdugo [aa], P. Berges [p], B. Bertucci [ah], B.L. Betev [aw],
S. Bhattacharya [k], M. Biasini [ah], A. Biland [aw], G.M. Bilei [ah], J.J. Blaising [d],
S.C. Blyth [ai], G.J. Bobbink [b], R. Bock [a], A. Böhm [a], L. Boldizsar [o], B. Borgia [r,ak],
D. Bourilkov [aw], M. Bourquin [t], S. Braccini [t], J.G. Branson [an], V. Brigljevic [aw],
I.C. Brock [ai], A. Buffini [q], A. Buijs [as], J.D. Burger [p], W.J. Burger [ah], J. Busenitz [ar],
A. Button [c], X.D. Cai [p], M. Campanelli [aw], M. Capell [p], G. Cara Romeo [j],
G. Carlino [ad], A.M. Cartacci [q], J. Casaus [aa], G. Castellini [q], F. Cavallari [ak],
N. Cavallo [ad], C. Cecchi [t], M. Cerrada [aa], F. Cesaroni [x], M. Chamizo [aa],
Y.H. Chang [ay], U.K. Chaturvedi [s], M. Chemarin [z], A. Chen [ay], G. Chen [h],
G.M. Chen [h], H.F. Chen [u], H.S. Chen [h], X. Chereau [d], G. Chiefari [ad], C.Y. Chien [e],
L. Cifarelli [am], F. Cindolo [j], C. Civinini [q], I. Clare [p], R. Clare [p], G. Coignet [d],
A.P. Colijn [b], N. Colino [aa], S. Costantini [i], F. Cotorobai [n], B. de la Cruz [aa],
A. Csilling [o], T.S. Dai [p], R. D'Alessandro [q], R. de Asmundis [ad], A. Degré [d],
K. Deiters [au], D. della Volpe [ad], P. Denes [aj], F. DeNotaristefani [ak], M. Diemoz [ak],
D. van Dierendonck [b], F. Di Lodovico [aw], C. Dionisi [r,ak], M. Dittmar [aw],
A. Dominguez [an], A. Doria [ad], M.T. Dova [s,1], D. Duchesneau [d], P. Duinker [b],
I. Duran [ao], S. Easo [ah], H. El Mamouni [z], A. Engler [ai], F.J. Eppling [p], F.C. Erné [b],
J.P. Ernenwein [z], P. Extermann [t], M. Fabre [au], R. Faccini [ak], M.A. Falagan [aa],
S. Falciano [ak], A. Favara [q], J. Fay [z], O. Fedin [al], M. Felcini [aw], T. Ferguson [ai],

F. Ferroni [ak], H. Fesefeldt [a], E. Fiandrini [ah], J.H. Field [t], F. Filthaut [r], P.H. Fisher [p],
I. Fisk [an], G. Forconi [p], L. Fredj [t], K. Freudenreich [aw], C. Furetta [ab],
Yu. Galaktionov [ac,p], S.N. Ganguli [k], P. Garcia-Abia [f], M. Gataullin [ag], S.S. Gau [m],
S. Gentile [ak], N. Gheordanescu [n], S. Giagu [ak], S. Goldfarb [w], J. Goldstein [l],
Z.F. Gong [u], A. Gougas [e], G. Gratta [ag], M.W. Gruenewald [i], R. van Gulik [b],
V.K. Gupta [aj], A. Gurtu [k], L.J. Gutay [at], D. Haas [f], B. Hartmann [a], A. Hasan [ae],
D. Hatzifotiadou [j], T. Hebbeker [i], A. Hervé [r], P. Hidas [o], J. Hirschfelder [ai],
W.C. van Hoek [af], H. Hofer [aw], H. Hoorani [ai], S.R. Hou [ay], G. Hu [e], I. Iashvili [av],
B.N. Jin [h], L.W. Jones [c], P. de Jong [r], I. Josa-Mutuberria [aa], R.A. Khan [s],
D. Kamrad [av], J.S. Kapustinsky [y], M. Kaur [s,2], M.N. Kienzle-Focacci [t], D. Kim [ak],
D.H. Kim [aq], J.K. Kim [aq], S.C. Kim [aq], W.W. Kinnison [y], A. Kirkby [ag], D. Kirkby [ag],
J. Kirkby [r], D. Kiss [o], W. Kittel [af], A. Klimentov [p,ac], A.C. König [af], A. Kopp [av],
I. Korolko [ac], V. Koutsenko [p,ac], R.W. Kraemer [ai], W. Krenz [a], A. Kunin [p,ac],
P. Lacentre [av,1,3], P. Ladron de Guevara [aa], I. Laktineh [z], G. Landi [q], C. Lapoint [p],
K. Lassila-Perini [aw], P. Laurikainen [v], A. Lavorato [am], M. Lebeau [r], A. Lebedev [p],
P. Lebrun [z], P. Lecomte [aw], P. Lecoq [r], P. Le Coultre [aw], H.J. Lee [i], J.M. Le Goff [r],
R. Leiste [av], E. Leonardi [ak], P. Levtchenko [al], C. Li [u], C.H. Lin [ay], W.T. Lin [ay],
F.L. Linde [b,r], L. Lista [ad], Z.A. Liu [h], W. Lohmann [av], E. Longo [ak], W. Lu [ag],
Y.S. Lu [h], K. Lübelsmeyer [a], C. Luci [r,ak], D. Luckey [p], L. Luminari [ak],
W. Lustermann [aw], W.G. Ma [u], M. Maity [k], G. Majumder [k], L. Malgeri [r],
A. Malinin [ac], C. Maña [aa], D. Mangeol [af], P. Marchesini [aw], G. Marian [ar,4], A. Marin [l],
J.P. Martin [z], F. Marzano [ak], G.G.G. Massaro [b], K. Mazumdar [k], R.R. McNeil [g],
S. Mele [r], L. Merola [ad], M. Meschini [q], W.J. Metzger [af], M. von der Mey [a],
D. Migani [j], A. Mihul [n], A.J.W. van Mil [af], H. Milcent [r], G. Mirabelli [ak], J. Mnich [r],
P. Molnar [i], B. Monteleoni [q], R. Moore [c], T. Moulik [k], R. Mount [ag], F. Muheim [t],
A.J.M. Muijs [b], S. Nahn [p], M. Napolitano [ad], F. Nessi-Tedaldi [aw], H. Newman [ag],
T. Niessen [a], A. Nippe [w], A. Nisati [ak], H. Nowak [av], Y.D. Oh [aq], G. Organtini [ak],
R. Ostonen [v], S. Palit [m], C. Palomares [aa], D. Pandoulas [a], S. Paoletti [ak], P. Paolucci [ad],
H.K. Park [ai], I.H. Park [aq], G. Pascale [ak], G. Passaleva [r], S. Patricelli [ad], T. Paul [m],
M. Pauluzzi [ah], C. Paus [r], F. Pauss [aw], D. Peach [r], Y.J. Pei [a], S. Pensotti [ab],
D. Perret-Gallix [d], B. Petersen [af], S. Petrak [i], A. Pevsner [e], D. Piccolo [ad], M. Pieri [q],
P.A. Piroué [aj], E. Pistolesi [ab], V. Plyaskin [ac], M. Pohl [aw], V. Pojidaev [ac,q],
H. Postema [p], J. Pothier [r], N. Produit [t], D. Prokofiev [al], J. Quartieri [am],
G. Rahal-Callot [aw], N. Raja [k], P.G. Rancoita [ab], M. Rattaggi [ab], G. Raven [an],
P. Razis [ae], D. Ren [aw], M. Rescigno [ak], S. Reucroft [m], T. van Rhee [as], S. Riemann [av],
K. Riles [c], A. Robohm [aw], J. Rodin [ar], B.P. Roe [c], L. Romero [aa], S. Rosier-Lees [d],
S. Roth [a], J.A. Rubio [r], D. Ruschmeier [i], H. Rykaczewski [aw], J. Salicio [r],
E. Sanchez [aa], M.P. Sanders [af], M.E. Sarakinos [v], C. Schäfer [a], V. Schegelsky [al],

S. Schmidt-Kaerst [a], D. Schmitz [a], N. Scholz [aw], H. Schopper [ax],
D.J. Schotanus [af], J. Schwenke [a], G. Schwering [a], C. Sciacca [ad], D. Sciarrino [t],
L. Servoli [ah], S. Shevchenko [ag], N. Shivarov [ap], V. Shoutko [ac], J. Shukla [y],
E. Shumilov [ac], A. Shvorob [ag], T. Siedenburg [a], D. Son [aq], B. Smith [p],
P. Spillantini [q], M. Steuer [p], D.P. Stickland [aj], A. Stone [g], H. Stone [aj],
B. Stoyanov [ap], A. Straessner [a], K. Sudhakar [k], G. Sultanov [s], L.Z. Sun [u],
G.F. Susinno [t], H. Suter [aw], J.D. Swain [s], X.W. Tang [h], L. Tauscher [f], L. Taylor [m],
C. Timmermans [af], Samuel C.C. Ting [p], S.M. Ting [p], S.C. Tonwar [k], J. Tóth [o],
C. Tully [aj], K.L. Tung [h], Y. Uchida [p], J. Ulbricht [aw], E. Valente [ak],
G. Vesztergombi [o], I. Vetlitsky [ac], G. Viertel [aw], M. Vivargent [d], S. Vlachos [f],
H. Vogel [ai], H. Vogt [av], I. Vorobiev [r,ac], A.A. Vorobyov [al], A. Vorvolakos [ae],
M. Wadhwa [f], W. Wallraff [a], J.C. Wang [p], X.L. Wang [u], Z.M. Wang [u], A. Weber [a],
S.X. Wu [p], S. Wynhoff [a], J. Xu [l], Z.Z. Xu [u], B.Z. Yang [u], C.G. Yang [h],
H.J. Yang [h], M. Yang [h], J.B. Ye [u], S.C. Yeh [az], J.M. You [ai], An. Zalite [al],
Yu. Zalite [al], P. Zemp [aw], Y. Zeng [a], Z.P. Zhang [u], B. Zhou [l], G.Y. Zhu [h],
R.Y. Zhu [ag], A. Zichichi [j,r,s], F. Ziegler [av], G. Zilizi [ar,4]

[a] *I. Physikalisches Institut, RWTH, D-52056 Aachen, FRG [5]*
III. Physikalisches Institut, RWTH, D-52056 Aachen, FRG [5]
[b] *National Institute for High Energy Physics, NIKHEF, and University of Amsterdam, NL-1009 DB Amsterdam, The Netherlands*
[c] *University of Michigan, Ann Arbor, MI 48109, USA*
[d] *Laboratoire d'Annecy-le-Vieux de Physique des Particules, LAPP,IN2P3-CNRS, BP 110, F-74941 Annecy-le-Vieux CEDEX, France*
[e] *Johns Hopkins University, Baltimore, MD 21218, USA*
[f] *Institute of Physics, University of Basel, CH-4056 Basel, Switzerland*
[g] *Louisiana State University, Baton Rouge, LA 70803, USA*
[h] *Institute of High Energy Physics, IHEP, 100039 Beijing, China [6]*
[i] *Humboldt University, D-10099 Berlin, FRG [5]*
[j] *University of Bologna and INFN-Sezione di Bologna, I-40126 Bologna, Italy*
[k] *Tata Institute of Fundamental Research, Bombay 400 005, India*
[l] *Boston University, Boston, MA 02215, USA*
[m] *Northeastern University, Boston, MA 02115, USA*
[n] *Institute of Atomic Physics and University of Bucharest, R-76900 Bucharest, Romania*
[o] *Central Research Institute for Physics of the Hungarian Academy of Sciences, H-1525 Budapest 114, Hungary [7]*
[p] *Massachusetts Institute of Technology, Cambridge, MA 02139, USA*
[q] *INFN Sezione di Firenze and University of Florence, I-50125 Florence, Italy*
[r] *European Laboratory for Particle Physics, CERN, CH-1211 Geneva 23, Switzerland*
[s] *World Laboratory, FBLJA Project, CH-1211 Geneva 23, Switzerland*
[t] *University of Geneva, CH-1211 Geneva 4, Switzerland*
[u] *Chinese University of Science and Technology, USTC, Hefei, Anhui 230 029, China [6]*
[v] *SEFT, Research Institute for High Energy Physics, P.O. Box 9, SF-00014 Helsinki, Finland*
[w] *University of Lausanne, CH-1015 Lausanne, Switzerland*
[x] *INFN-Sezione di Lecce and Universitá Degli Studi di Lecce, I-73100 Lecce, Italy*
[y] *Los Alamos National Laboratory, Los Alamos, NM 87544, USA*
[z] *Institut de Physique Nucléaire de Lyon, IN2P3-CNRS, Université Claude Bernard, F-69622 Villeurbanne, France*
[aa] *Centro de Investigaciones Energeticas, Medioambientales y Tecnologicas, CIEMAT, E-28040 Madrid, Spain [8]*
[ab] *INFN-Sezione di Milano, I-20133 Milan, Italy*
[ac] *Institute of Theoretical and Experimental Physics, ITEP, Moscow, Russia*
[ad] *INFN-Sezione di Napoli and University of Naples, I-80125 Naples, Italy*
[ae] *Department of Natural Sciences, University of Cyprus, Nicosia, Cyprus*
[af] *University of Nijmegen and NIKHEF, NL-6525 ED Nijmegen, The Netherlands*

[ag] *California Institute of Technology, Pasadena, CA 91125, USA*
[ah] *INFN-Sezione di Perugia and Universitá Degli Studi di Perugia, I-06100 Perugia, Italy*
[ai] *Carnegie Mellon University, Pittsburgh, PA 15213, USA*
[aj] *Princeton University, Princeton, NJ 08544, USA*
[ak] *INFN-Sezione di Roma and University of Rome, ''La Sapienza'', I-00185 Rome, Italy*
[al] *Nuclear Physics Institute, St. Petersburg, Russia*
[am] *University and INFN, Salerno, I-84100 Salerno, Italy*
[an] *University of California, San Diego, CA 92093, USA*
[ao] *Dept. de Fisica de Particulas Elementales, Univ. de Santiago, E-15706 Santiago de Compostela, Spain*
[ap] *Bulgarian Academy of Sciences, Central Lab. of Mechatronics and Instrumentation, BU-1113 Sofia, Bulgaria*
[aq] *Center for High Energy Physics, Adv. Inst. of Sciences and Technology, 305-701 Taejon, South Korea*
[ar] *University of Alabama, Tuscaloosa, AL 35486, USA*
[as] *Utrecht University and NIKHEF, NL-3584 CB Utrecht, The Netherlands*
[at] *Purdue University, West Lafayette, IN 47907, USA*
[au] *Paul Scherrer Institut, PSI, CH-5232 Villigen, Switzerland*
[av] *DESY-Institut für Hochenergiephysik, D-15738 Zeuthen, FRG*
[aw] *Eidgenössische Technische Hochschule, ETH Zürich, CH-8093 Zürich, Switzerland*
[ax] *University of Hamburg, D-22761 Hamburg, FRG*
[ay] *National Central University, Chung-Li, Taiwan, ROC*
[az] *Department of Physics, National Tsing Hua University, Taiwan, China*

Abstract

A search for the lightest neutral scalar and neutral pseudoscalar Higgs bosons in the Minimal Supersymmetric Standard Model is performed on data collected at LEP by the L3 detector at center-of-mass energies $130\,\mathrm{GeV} \leq \sqrt{s} \leq 183\,\mathrm{GeV}$. No significant excess of events is observed. Limits on the masses of the lightest neutral and pseudoscalar Higgs bosons are given as a function of $\tan\beta$. Lower mass limits at the 95% confidence level are set at $m_\mathrm{h} > 70.7\,\mathrm{GeV}$ and $m_\mathrm{A} > 71.0\,\mathrm{GeV}$.
© 1998 Elsevier Science B.V. All rights reserved.

1. Introduction

In the Standard Model [1] (SM), one Higgs doublet [2] gives rise to one neutral, scalar particle, the

Higgs boson. A lower limit on its mass has been set by L3 at 87.6 GeV, mainly from a search for the process $e^+e^- \to Z^* \to HZ$ [3]. In contrast to the SM, the Minimal Supersymmetric Standard Model [4] (MSSM) requires two Higgs doublets, which give rise to a charged scalar pair, two neutral scalars, the lightest of which is called h, and a neutral pseudoscalar, A. We consider the two production mechanisms most important at these LEP center-of-mass energies:

$$e^+e^- \to Z^* \to hZ \tag{1}$$

$$e^+e^- \to Z^* \to hA. \tag{2}$$

The rate for the Higgs-strahlung process (1) is, in general, reduced compared to the similar Standard Model reaction, but this is compensated by the additional pair-production process (2).

Previous searches for the h and A bosons have been reported by L3 [5] and other experiments [6]. In

this letter, we present the results of the search for the production of h and A using a data sample with an integrated luminosity of 88.3 pb^{-1} collected at center-of-mass energies 130 GeV $\leq \sqrt{s} \leq$ 183 GeV.

2. Data and Monte Carlo samples

The data were collected using the L3 detector [7] at LEP from 1995 to 1997. The integrated luminosities are 6.1, 5.9, 10.8, 10.2 and 55.3 pb^{-1} at the average center-of-mass energies of 130.3, 136.3, 161.3, 172.3 and 182.7 GeV, respectively.

The signal cross sections and branching ratios are calculated using the HZHA generator [8]. For the efficiency studies, Monte Carlo samples of Higgs events are generated using PYTHIA [9]. For the background studies, the following Monte Carlo programs are used: PYTHIA ($e^+e^- \to q\bar{q}$), KORALW [10] ($e^+e^- \to W^+W^-$), KORALZ [11] ($e^+e^- \to \tau^+\tau^-$), PYTHIA and PHOJET [12] ($e^+e^- \to e^+e^-q\bar{q}$), and EXCALIBUR [13] ($e^+e^- \to f\bar{f}'f\tilde{f}'$). The number of simulated background events for the most important background channels is typically 100 times the number of collected data events. The Monte Carlo signals are 300 times the number of events expected to be observed with these luminosities.

The L3 detector response is simulated using the GEANT 3.15 program [14], which takes into account the effects of energy loss, multiple scattering and showering in the detector. The GHEISHA program [15] is used to simulate hadronic interactions in the detector.

3. Analysis procedures

The search for hA and hZ production is carried out using three different sets of MSSM parameters, as suggested in Ref. [16]. This choice of parameters makes use of the Grand Unification assumption [17]. This assumption has little impact on the masses of the Higgs bosons, but it reduces the number of free parameters in the MSSM. The free parameters are chosen to be the ratio of the two Higgs vacuum expectation values, $\tan\beta$; the pseudoscalar Higgs mass, m_A; the gaugino mass parameter, M_2; the scalar fermion mass, m_0; the scalar quark mixing

mass, A; and the Higgs mass parameter, μ. The three sets of MSSM parameters used in this letter are called "minimal mixing", where A is zero and $\mu = -0.1$ TeV; "typical mixing", $A = 1$ TeV and $\mu = -1$ TeV; and "maximal mixing", $A = \sqrt{6}$ TeV and $\mu = -0.1$ TeV. For all three mixing scenarios $M_2 = m_0 = 1$ TeV and the mass of the top quark, m_t, is taken to be $m_t = 175$ GeV [18]. Finally, a scan over the two remaining independent parameters, $\tan\beta$ and m_A, is performed in each mixing scheme for the ranges

$$1 \leq \tan\beta \leq 50$$

$$30\,\text{GeV} \leq m_A \leq 1000\,\text{GeV}\,.$$

Values of $\tan\beta$ and m_A outside of these ranges are not considered since the sensitivity to the signal drops for $\tan\beta < 1$ and for values of $m_A < 30$ GeV the analysis is complicated by the possibility of $h \to AA$ decays. In addition, these low masses have been previously excluded [5,6] for these choices of MSSM parameters.

Because the relative production rate of the two complementary processes, $e^+e^- \to Z^* \to hA$ and $e^+e^- \to Z^* \to hZ$, varies over the range of MSSM parameters considered, it is important to devise an analysis scheme that has good sensitivity to both channels for a broad range of these parameters. In the case of hZ decay, four event topologies representing approximately 98% of the decay modes are considered: $q\bar{q}q\bar{q}$, $q\bar{q}\nu\bar{\nu}$, $q\bar{q}\ell^+\ell^-$ ($\ell = e,\mu,\tau$) and $\tau^+\tau^-q\bar{q}$. The analyses of the $q\bar{q}\nu\bar{\nu}$ and $q\bar{q}\ell^+\ell^-$ ($\ell = e,\mu$) channels were taken from the Standard Model Higgs search [3]. The hZ analyses are optimized for $h \to b\bar{b}$, but the efficiencies for the small contributions from the decay modes $h \to c\bar{c},gg$ are also considered. The hZ $\to b\bar{b}q\bar{q}$ and hZ $\to b\bar{b}\tau^+\tau^-$ ($\tau^+\tau^-q\bar{q}$) analyses used in this letter achieve similar performances to the corresponding analyses used in the Standard Model Higgs search, which are described in detail in Ref. [19].

There are two event topologies considered for the hA channel, which generally make up approximately 97% of the available decay modes for these ranges of MSSM parameters: hA $\to b\bar{b}b\bar{b}$ and hA $\to b\bar{b}\tau^+\tau^-$ ($\tau^+\tau^-b\bar{b}$). These topologies are very similar to their hZ counterparts, but the Z-mass constraint cannot be used and, on average, the hA events are more likely to contain b hadrons.

The analyses of the hA and hZ channels are performed in three stages. First, a high-multiplicity hadronic event selection is applied. This greatly reduces background events with large missing energy and low multiplicity while maintaining a high signal efficiency over a broad range of possible Higgs masses. Second, a set of cuts tailored to the specific Higgs decay in question is chosen using an automated optimization procedure [19,20]. These cuts are optimized for each center-of-mass energy. Third, a discriminating variable is built for each analysis, which depends on the mass hypothesis and relative production rates of hA and hZ. The spectrum of this discriminant is recomputed for each point in the $(\tan\beta, m_A)$ scan and it is used in the likelihood calculation which tests for the presence of a signal.

The b-tagging variable plays a large role in the calculation of this discriminant. The neural network b-tag [21] for each hadronic jet is calculated from inputs including the measured decay lengths of particles in three dimensions, information about prompt leptons and jet shape variables. The event b-tag variable, $B_{\text{tag}}^{\text{event}}$, is then defined to be the negative-logarithm of the probability that all the hadronic jets in the event are consistent with jets containing no b hadrons.

3.1. The $hA \to b\bar{b}b\bar{b}$ and $hZ \to b\bar{b}q\bar{q}$ channels

The signature of both the $hA \to b\bar{b}b\bar{b}$ and $hZ \to b\bar{b}q\bar{q}$ decay modes is four high-multiplicity hadronic jets and the presence of b hadron decay products. The dominant backgrounds come from $q\bar{q}$ production and hadronic decays of W-pairs. In the case of $hA \to b\bar{b}b\bar{b}$, the identification of b hadrons plays an especially important role. Both analyses proceed in three stages.

First, a high-multiplicity hadronic event preselection common to both channels is made at all center-of-mass energies. At least 15 tracks and 45 calorimetric clusters are required, the visible energy, E_{vis}, must exceed $0.6\sqrt{s}$ and radiative returns to the Z-resonance are rejected. Events passing the preselection are then forced to have four jets using the DURHAM [22] clustering algorithm and a kinematic fit requiring 4-momentum conservation (4C) is performed.

The second stage of the analyses optimizes the signal sensitivity by automatically adjusting a set of

cuts to maximize the average confidence level using the technique described in Ref. [19]. The values of the optimized cuts for all the center-of-mass energies are discussed in detail in Ref. [23]. As an example, we describe the cuts for $\sqrt{s} = 183$ GeV since these data contribute the most to the sensitivity of the search due to the high center-of-mass energy and large integrated luminosity. The optimized cuts at the lower center-of-mass energies are similar to those of the $\sqrt{s} = 183$ GeV, but take into account the different background conditions and signal cross sections.

For the $hZ \to b\bar{b}q\bar{q}$ and $hA \to b\bar{b}b\bar{b}$ analyses, the following mass variables are defined:

$$
\chi_{hZ} = \log\Big(\text{Prob}\big(\min\big((\Sigma_i - (m_Z + m_h))^2 w_\Sigma
$$
$$
+ (\Delta_i - |m_Z - m_h|)^2 w_\Delta\big)\big)\Big)
$$
$$
\chi_{hA} = \log\Big(\text{Prob}\big(\min\big((\Sigma_i - (m_A + m_h))^2 w_\Sigma
$$
$$
+ (\Delta_i - |m_A - m_h|)^2 w_\Delta\big)\big)\Big) , \qquad (3)
$$

where Σ_i and Δ_i are the sum and difference, respectively, of the ith dijet masses of one the three jet pairings. The weights w_Σ and w_Δ are respectively $1/(4\,\text{GeV})^2$ and $1/(6\,\text{GeV})^2$ reflecting the typical mass resolutions, and Prob is the probability of a χ^2 with two degrees of freedom. In the $hZ \to b\bar{b}q\bar{q}$ selection, the mass variable, χ_{hZ}, must be $\chi_{hZ} > -13.3$ and in the $hA \to b\bar{b}b\bar{b}$ selection, $\chi_{hA} > -6.1$. This rejects events with dijet mass combinations far away from the Higgs mass hypothesis. The Y_{cut} parameter in the DURHAM scheme, Y_{34}^{D}, ensures the four-jet nature of the selected events and must be $Y_{34}^{\text{D}} > 0.0044$ in the $hZ \to b\bar{b}q\bar{q}$ analysis and $Y_{34}^{\text{D}} > 0.0030$ in the $hA \to b\bar{b}b\bar{b}$ analysis. A cut on the maximum energy difference between any two jets rejects events with gluonic jets and is chosen to be $\max(\Delta E_{\text{jet}}) < 0.22\sqrt{s}$ for $hZ \to b\bar{b}q\bar{q}$ and $\max(\Delta E_{\text{jet}}) < 0.32\sqrt{s}$ for $hA \to b\bar{b}b\bar{b}$. To further reject $q\bar{q}$ background, the minimum dijet mass is required to be inside a window of $0.14\sqrt{s} < \min(M_i) < 0.66\sqrt{s}$ for the $hZ \to b\bar{b}q\bar{q}$ selection and $0.09\sqrt{s} < \min(M_i) < 0.78\sqrt{s}$ for the $hA \to b\bar{b}b\bar{b}$ selection. The final and most important optimized cut is on $B_{\text{tag}}^{\text{event}}$, which mainly rejects W-pair decays. In the $hZ \to b\bar{b}q\bar{q}$ analysis, $B_{\text{tag}}^{\text{event}}$ needs to be $B_{\text{tag}}^{\text{event}} > 0.06$ and in the $hA \to b\bar{b}b\bar{b}$ analysis $B_{\text{tag}}^{\text{event}} > 0.67$.

The most discriminating of these variables are shown in Fig. 1 for the data and Monte Carlo at $\sqrt{s} = 183\,\text{GeV}$ after the preselection but before the optimized cuts have been applied. The signal efficiencies and the number of accepted events after the preselection and after passing either set of the optimized cuts (except the cut on the mass variable) for $hZ \to b\bar{b}q\bar{q}$ or $hA \to b\bar{b}b\bar{b}$ are shown in Tables 1 and 2 for the data and Monte Carlo background.

Events passing the optimized cuts are then categorized: 1) those that pass only the hZ cuts; 2) those that pass only the hA cuts; and 3) those that pass both sets of cuts. Category (1) is called the $hZ_{b\bar{b}q\bar{q}}$ analysis and category (2) the $hA_{b\bar{b}b\bar{b}}$ analysis. Events in category (3) are split into two separate samples by choosing the most likely production hypothesis based on the probability of the χ^2 of the mass hypothesis and the relative production rates. If $\sigma_{hA \to b\bar{b}b\bar{b}}$-
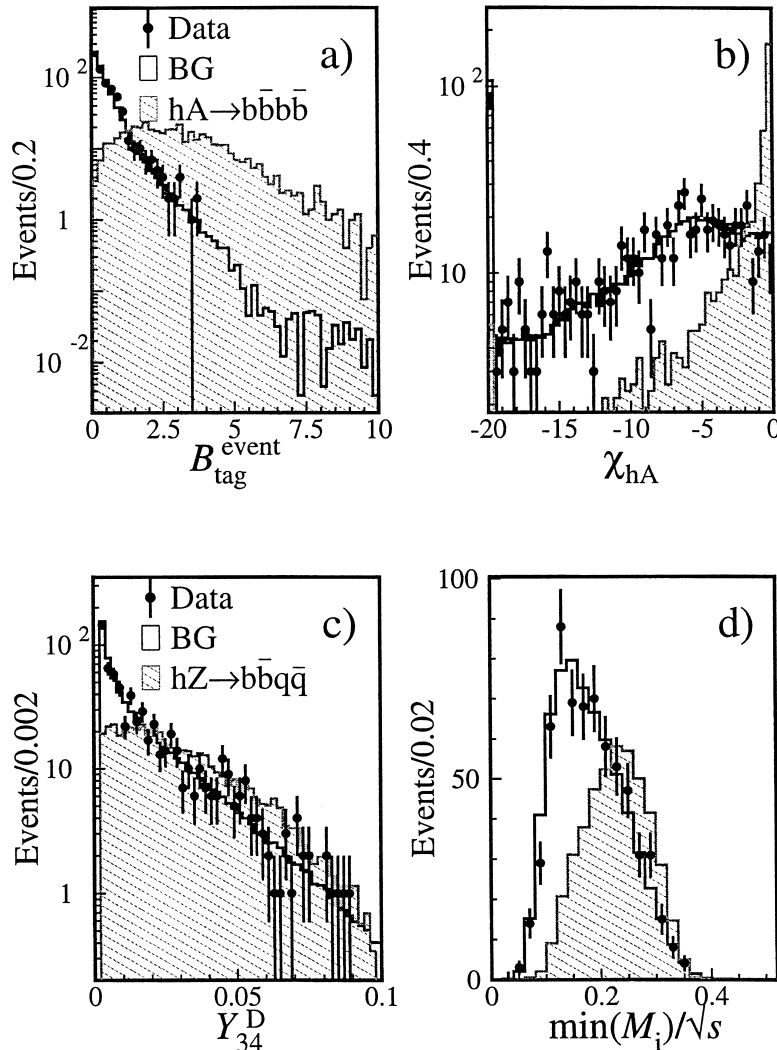
Fig. 1. Distributions of the most important variables in the $hA \to b\bar{b}b\bar{b}$ and $hZ \to b\bar{b}q\bar{q}$ analyses. In the plots, the points are the $\sqrt{s} = 183\,\text{GeV}$ data, the solid histograms are the Monte Carlo backgrounds and the superimposed hatched histograms are the hA ($m_A = m_h = 70\,\text{GeV}$) or hZ ($m_h = 85\,\text{GeV}$) signals normalized to efficiency times 500. The distributions are shown after preselection, but before optimized cuts: **a)** Event b-tag, $B_{\text{tag}}^{\text{event}}$, for the $hA \to b\bar{b}b\bar{b}$ analysis; **b)** Mass variable, χ_{hA}, for the $hA \to b\bar{b}b\bar{b}$ analysis; **c)** Y_{34}^{D} for the $hZ \to b\bar{b}q\bar{q}$ analysis; and **d)** Minimum normalized dijet mass, $\min(M_i/\sqrt{s})$, for the $hZ \to b\bar{b}q\bar{q}$ analysis.

Table 1

The effects of the preselection and optimized cuts at the five center-of-mass energies. On the left hand side are the signal efficiencies, the number expected background events, N_{bg}, and the number of data events, N_{data}, passing the common hA and hZ preselection in the four-jet channel. On the right hand side, the same is shown for events passing either set of the optimized cuts. The signal efficiencies, $\epsilon_{hA \to b\bar{b}b\bar{b}}$, are for the following center-of-mass energies and signal masses: $\sqrt{s} = 130 - 136\,\text{GeV}$, $m_A = m_h = 50\,\text{GeV}$; $\sqrt{s} = 161 - 172\,\text{GeV}$, $m_A = m_h = 60\,\text{GeV}$; and $\sqrt{s} = 183\,\text{GeV}$, $m_A = m_h = 70\,\text{GeV}$. The efficiencies, $\epsilon_{hZ \to b\bar{b}q\bar{q}}$, are for: $\sqrt{s} = 161 - 172\,\text{GeV}$, $m_h = 71\,\text{GeV}$; and $\sqrt{s} = 183\,\text{GeV}$, $m_h = 85\,\text{GeV}$. At this stage of the analysis, the acceptances are independent of $\tan\beta$.

$\sqrt{s}$ (GeV)	Preselection				Optimized Cuts hA$_{b\bar{b}b\bar{b}}$ or hZ$_{b\bar{b}q\bar{q}}$			
	$\epsilon_{hA \to b\bar{b}b\bar{b}}$	$\epsilon_{hZ \to b\bar{b}q\bar{q}}$	N_{bg}	N_{data}	$\epsilon_{hA \to b\bar{b}b\bar{b}}$	$\epsilon_{hZ \to b\bar{b}q\bar{q}}$	N_{bg}	N_{data}
130	0.92	–	148.9	148	0.66	–	20.1	19
136	0.92	–	112.0	118	0.70	–	9.5	11
161	0.94	0.95	134.5	128	0.85	0.75	25.2	14
172	0.95	0.97	193.7	186	0.83	0.89	84.0	80
183	0.89	0.91	655.6	652	0.78	0.84	380.5	376

Prob($\chi^2(m_A, m_h)$) $> \sigma_{hZ \to b\bar{b}q\bar{q}}$Prob($\chi^2(m_Z, m_h)$), then the event is classified as hA $\to$ b$\bar{b}$b$\bar{b}$ and this analysis is called hA$'_{b\bar{b}b\bar{b}}$, otherwise it is classified as hZ $\to$ b$\bar{b}$q$\bar{q}$ and called hZ$'_{b\bar{b}q\bar{q}}$.

In the last stage of the hZ$_{b\bar{b}q\bar{q}}$, hA$_{b\bar{b}b\bar{b}}$, hZ$'_{b\bar{b}q\bar{q}}$ and hA$'_{b\bar{b}b\bar{b}}$ analyses, the discriminating variables, $F(m_Z, m_h)$ and $F(m_A, m_h)$, are computed. These variables are the weighted combination of the B_{tag}^{event} and χ probabilities:

$$F(m_x, m_h) = -\log\left(\frac{\omega P_B^{1/\omega} P_\chi - P_B P_\chi^\omega}{\omega - 1}\right), \qquad (4)$$

where m_x is either m_Z or m_A, P_B and P_χ are the probabilities of B_{tag}^{event} and χ each being consistent with their respective background distributions, and ω is a weighting parameter that is optimized for each analysis. For the hZ$_{b\bar{b}q\bar{q}}$ and hZ$'_{b\bar{b}q\bar{q}}$ analyses, the mass variable $\chi = \chi_{hZ}$ is used and F is a function of the m_h hypothesis, $F(m_Z, m_h)$. Conversely, for hA$_{b\bar{b}b\bar{b}}$ and hA$'_{b\bar{b}b\bar{b}}$, $\chi = \chi_{hA}$ is used and F depends on the m_A and m_h mass hypothesis, $F(m_A, m_h)$. Spectra of $F(m_A, m_h)$ for the $\sqrt{s} = 183\,\text{GeV}$ data can be seen in Fig. 2a and Fig. 2b, for the hA$_{b\bar{b}b\bar{b}}$ and hA$'_{b\bar{b}b\bar{b}}$ analyses with a mass hypothesis of $m_A = m_h = 70\,\text{GeV}$ for typical mixing. In Fig. 2c and Fig. 2d, we show the spectra for $F(m_Z, m_h)$ in the hZ$_{b\bar{b}q\bar{q}}$ and hZ$'_{b\bar{b}q\bar{q}}$ analyses for the $m_h = 85\,\text{GeV}$ mass hypothesis in the typical mixing scheme.

The discriminant variable, F, is recomputed at each $(\tan\beta, m_A)$ point in the scan for the mixing scenario under consideration. Because of the cut on the χ variables, the number of accepted data, Monte Carlo background and signal events is different at each scanned point.

3.2. hA $\to$ b$\bar{b}\tau^+\tau^-$ ($\tau^+\tau^-$b$\bar{b}$), hZ $\to$ b$\bar{b}\tau^+\tau^-$ and hZ $\to$ $\tau^+\tau^-$q$\bar{q}$ channels

The signatures of these events are a pair of high-energy taus accompanied by two hadronic jets. The

Table 2

Events passing the optimized b$\bar{b}\tau^+\tau^-$ selection. The efficiencies, $\epsilon_{hA \to b\bar{b}\tau^+\tau^-}$, are for the following center-of-mass energies and signal masses: $\sqrt{s} = 133\,\text{GeV}$, $m_A = m_h = 50\,\text{GeV}$; $\sqrt{s} = 161 - 172\,\text{GeV}$, $m_A = m_h = 60\,\text{GeV}$; and $\sqrt{s} = 183\,\text{GeV}$, $m_A = m_h = 70\,\text{GeV}$. The efficiencies, $\epsilon_{hZ \to b\bar{b}\tau^+\tau^-}$ and $\epsilon_{hZ \to \tau^+\tau^-q\bar{q}}$, are for signal masses: $\sqrt{s} = 161 - 172\,\text{GeV}$, $m_h = 70\,\text{GeV}$; and $\sqrt{s} = 183\,\text{GeV}$, $m_h = 85\,\text{GeV}$. The last two columns are the number of Monte Carlo background events, N_{bg}, and number of data events, N_{data}, surviving the cuts

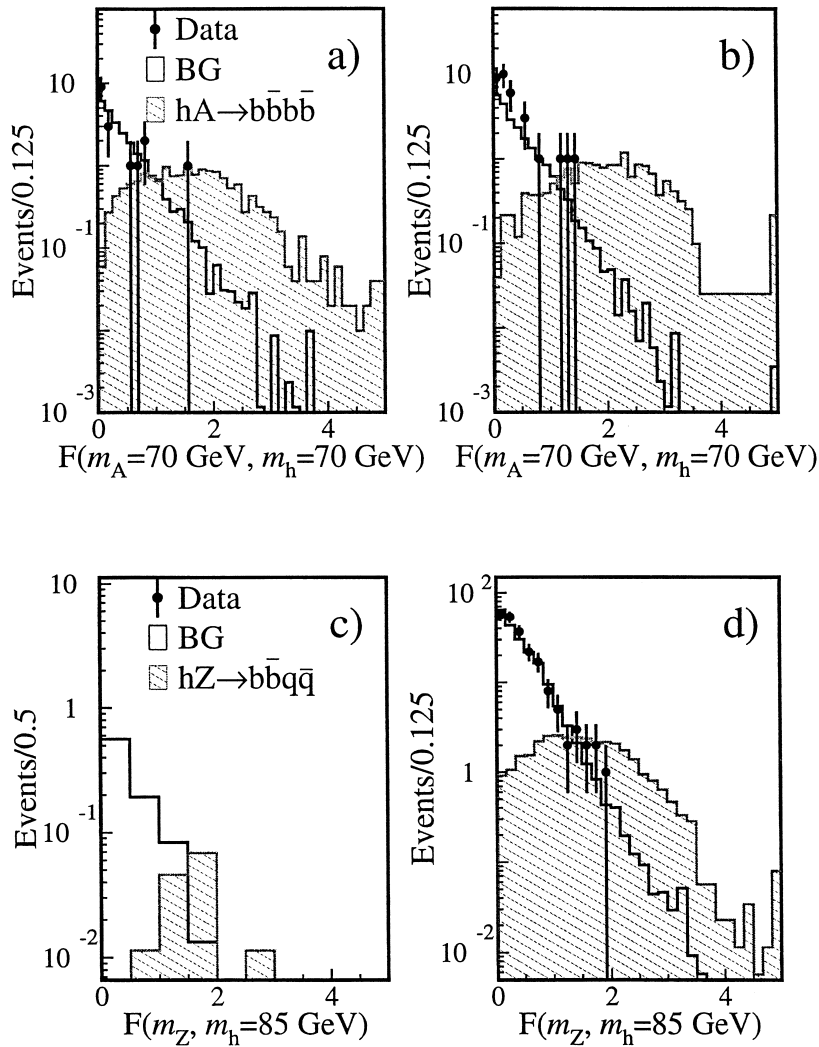| $\sqrt{s}$ (GeV)	$\epsilon_{hA \to b\bar{b}\tau^+\tau^-}$	$\epsilon_{hZ \to b\bar{b}\tau^+\tau^-}$	$\epsilon_{hZ \to \tau^+\tau^-q\bar{q}}$	N_{bg}	N_{data}
133	0.27	–	–	2.7	4
161	0.32	0.30	0.28	1.8	2
172	0.33	0.27	0.28	4.2	3
183	0.32	0.27	0.30	14.0	17

Fig. 2. The discriminant, $F(m_A, m_h)$ and $F(m_Z, m_h)$, after the optimized cuts have been applied. Data are the points, the open histograms are Monte Carlo background and the superimposed hatched histograms are signal efficiency times 50: **a)** $hA_{b\bar{b}b\bar{b}}$ analysis at $\tan\beta = 50$, $m_A = m_h = 70$ GeV, typical mixing; **b)** same as (a) but for the $hA'_{b\bar{b}b\bar{b}}$ analysis; **c)** $hZ_{b\bar{b}q\bar{q}}$ analysis at $\tan\beta = 1$, $m_h = 85$ GeV, typical mixing; and **d)** same as (c) but for the $hZ'_{b\bar{b}q\bar{q}}$ analysis.

main backgrounds are $q\bar{q}$ production and four-jet W-pair decays. The identification criteria of hadronically and leptonically decaying taus are given in Ref. [24]. As in the $hA \to b\bar{b}b\bar{b}$ and $hZ \to b\bar{b}q\bar{q}$ selection, the analysis proceeds in three stages.

First, a preselection is made for high-multiplicity events with tau leptons. At least 5 tracks are required, the number of calorimetric clusters must be greater than 15 and at least two taus must be present.

Then, in the same spirit as the $hA \to b\bar{b}b\bar{b}$ and $hZ \to b\bar{b}q\bar{q}$ analyses, an automated procedure [20] is used to optimize cuts on visible energy, visible mass, effective center-of-mass energy, and cuts devoted to tau isolation for each center-of-mass energy.

The isolation and energy requirements for the taus are optimized to reduce contributions from semileptonic and hadronic decays of W-pairs and $q\bar{q}$ backgrounds. Energy clusters not belonging to the taus

are forced into two jets using the DURHAM scheme and a 4C kinematic fit is performed, which defines the dijet and ditau invariant masses, M_i and M_τ.

Finally, events passing the common set of optimized cuts are classified as either hA $\rightarrow$ b$\bar{\text{b}}\tau^+\tau^-(\tau^+\tau^-$ b$\bar{\text{b}}$), hZ $\rightarrow$ b$\bar{\text{b}}\tau^+\tau^-$ or hZ $\rightarrow \tau^+\tau^-$ q$\bar{\text{q}}$

by choosing the most likely production hypothesis based on the mass χ^2 variables and the relative production rates as in the hA $\rightarrow$ b$\bar{\text{b}}$b$\bar{\text{b}}$ and hZ $\rightarrow$ b$\bar{\text{b}}$q$\bar{\text{q}}$ analyses. The mass χ^2 variables are defined as in Eq. (3) but the weights, w_Σ and w_Δ, are $1/(5\,\text{GeV})^2$ and $1/(10\,\text{GeV})^2$, respectively, for the sum and dif-
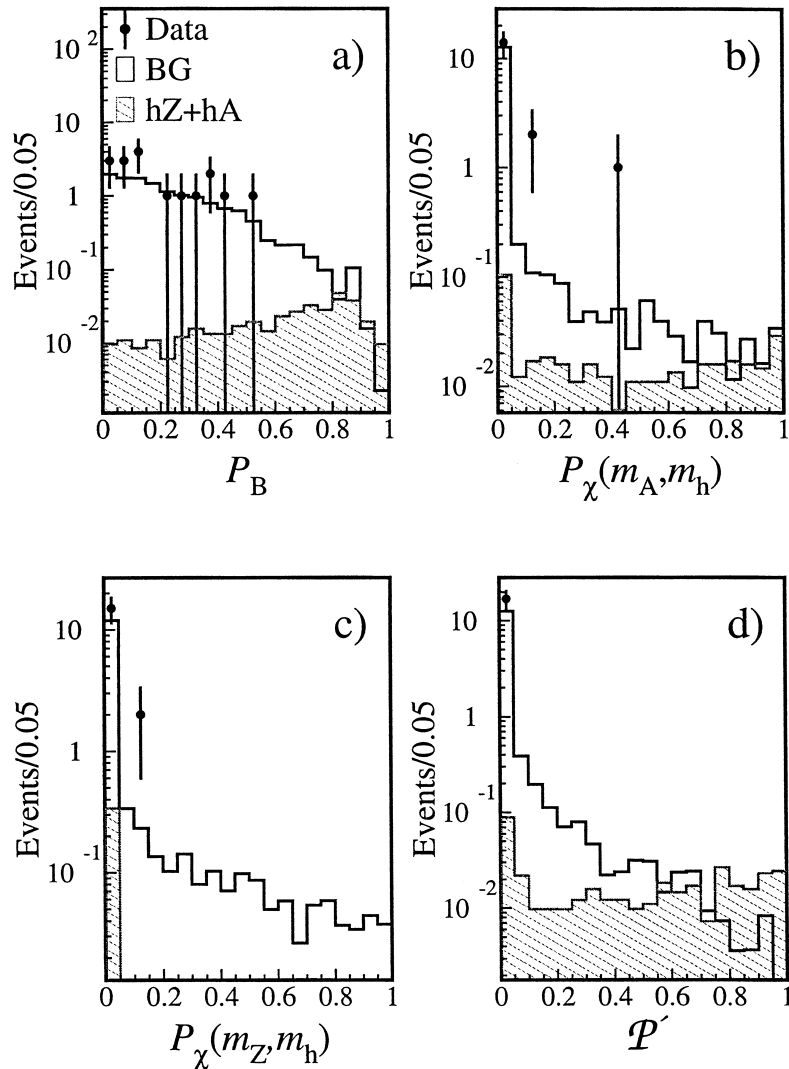
Fig. 3. Variables used in the calculation of the discriminant, $\mathscr{P}'$, for the hA $\rightarrow$ b$\bar{\text{b}}\tau^+\tau^-(\tau^+\tau^-$ b$\bar{\text{b}}$), hZ $\rightarrow$ b$\bar{\text{b}}\tau^+\tau^-$ and hZ $\rightarrow \tau^+\tau^-$ q$\bar{\text{q}}$ analyses at $\sqrt{s} = 183\,\text{GeV}$ for $(\tan\beta = 50, m_A = 70\,\text{GeV})$ for minimal mixing. The dots are data, the solid histograms are Monte Carlo and the hatched histograms are the inclusive signal hA $\rightarrow$ b$\bar{\text{b}}\tau^+\tau^-(\tau^+\tau^-$ b$\bar{\text{b}}$) + hZ $\rightarrow$ b$\bar{\text{b}}\tau^+\tau^-$ + hZ $\rightarrow \tau^+\tau^-$ q$\bar{\text{q}}$. **a)** The joint probability of both hadronic jets to be from b-decays. **b)** The mass probability to be signal. **c)** The mass probability for the hZ mass hypothesis. **d)** The discriminant, $\mathscr{P}'$, for the inclusive b$\bar{\text{b}}\tau^+\tau^-$ analysis.

ference of M_i and M_τ. The mass-dependent variable, $\mathscr{P} = 10^{-F}$, is defined using Eq. (4) with a weight of unity, which reduces to $\mathscr{P} = P_B P_\chi (1 - \ln(P_B P_\chi))$. Here, P_B and P_χ are the confidence levels that the b-tag from the two hadronic jets and mass χ^2 are consistent with their signal distributions. In the case of the $hZ \to \tau^+\tau^- q\bar{q}$ analysis, the b-tagging informa-

tion is not used and $\mathscr{P} = P_\chi$. The event is classified depending on the value of

$$\mathscr{P}' = \max\{\, \sigma_{hA \to b\bar{b}\tau^+\tau^-(\tau^+\tau^-b\bar{b})}\mathscr{P}(m_A, m_h),$$

$$\sigma_{hZ \to b\bar{b}\tau^+\tau^-}\mathscr{P}(m_Z, m_h),$$

$$\sigma_{hZ \to \tau^+\tau^-q\bar{q}}\mathscr{P}(m_Z, m_h)\}\,/\,\sigma_{b\tau}$$

where $\sigma_{b\tau}$ is the sum of these cross sections.
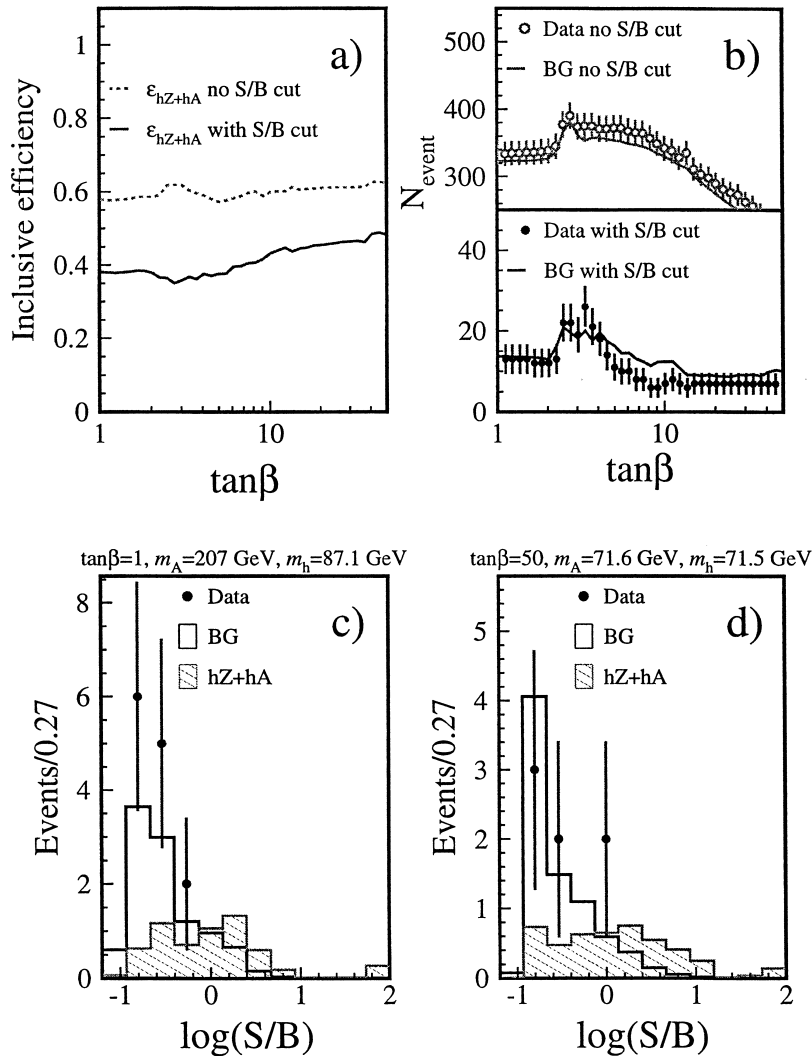
Fig. 4. Accepted events and signal efficiency near the average 95% CL limit as a function of $\tan\beta$ for maximal mixing. **a)** Inclusive efficiency for hA + hZ production before a signal-over-background cut (dotted line) and after a signal-over-background cut of 0.1 (solid line). **b)** Upper plot: Number of accepted data events (dots) and expected background (dotted line) before a signal-over-background cut. Lower plot: Number of data events (dots) and background (solid line) passing a signal-over-background cut of 0.1. **c)** Distribution for all analyses combined in bins of log(Signal/Background) for ($\tan\beta = 1, m_A = 207$ GeV), where hZ is the dominant production mode (open histogram is expected background, dots are data, hatched histogram is combined signal). **d)** Same as **(c)**, but for ($\tan\beta = 50, m_A = 71.6$ GeV), where hA is dominant.

Unlike the hA $\to$ b$\bar{b}$b$\bar{b}$ and hZ $\to$ b$\bar{b}$q$\bar{q}$ analyses, the events are not split into separate categories based on this decision, but are instead kept as one inclusive analysis. The discriminant, $\mathcal{P}'$, is recalculated at each $(\tan\beta, m_A)$ point in the scan for each mixing scenario. The spectrum for $\mathcal{P}'$ at $(\tan\beta = 50, m_A = 70\,\text{GeV})$ is shown in Fig. 3 for the $\sqrt{s} = 183\,\text{GeV}$ data, Monte Carlo background and an inclusive sig-
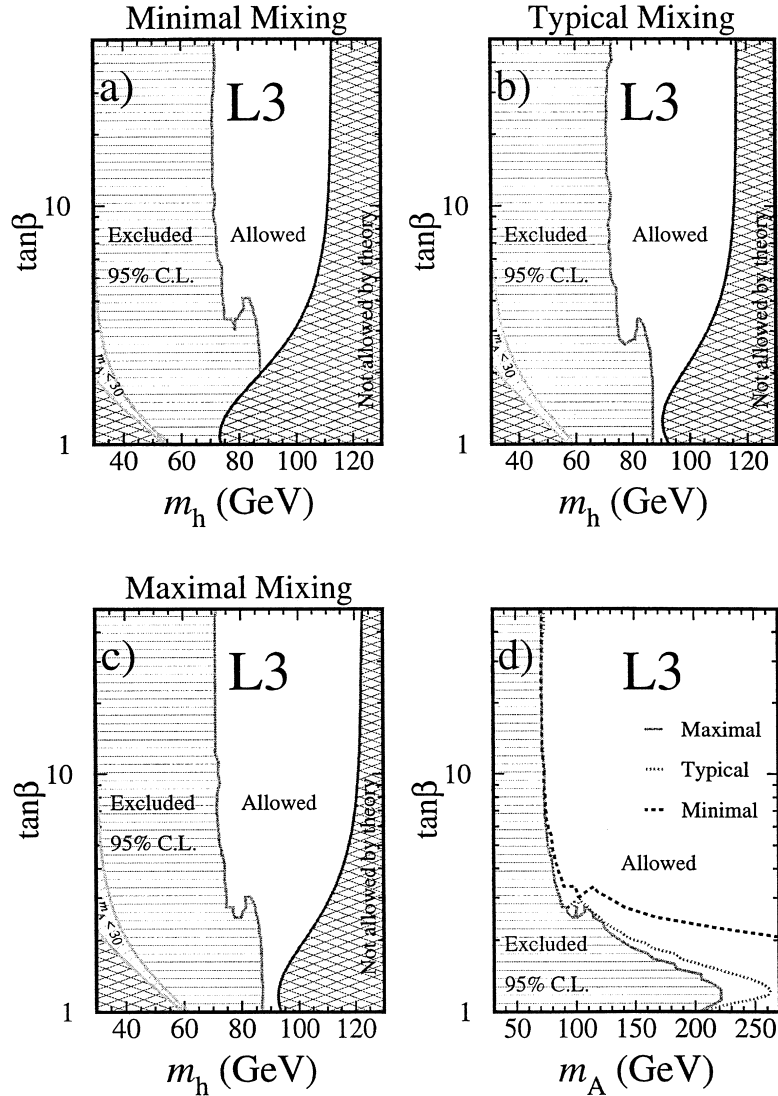
Fig. 5. Exclusion plots of the Higgs mass versus $\tan\beta$ at the 95% CL from the data collected at $\sqrt{s} = 130 - 183\,\text{GeV}$. In all the plots, the area shaded by horizontal lines is the 95% CL exclusion; the white area is the non-excluded region; the cross-hatched area is disallowed by theory and the area in the lower left hand corner of plots a,b and c between the 95% exclusion and the theoretically excluded regions represents the lower boundary of the scan over m_A which starts at 30 GeV. **a)** 95% CL exclusion of m_h versus $\tan\beta$ in the minimal mixing scenario. **b)** Same as (a) but for typical mixing. **c)** Same as (a,b) but for maximal mixing. **d)** 95% CL exclusion of m_A versus $\tan\beta$ in the three mixing scenarios. The solid line is the maximal mixing exclusion, the dotted line is typical mixing, and the dashed lined is minimal mixing.

nal of $hA \to b\bar{b}\tau^+\tau^-(\tau^+\tau^-b\bar{b}) + hZ \to b\bar{b}\tau^+\tau^- + hZ \to \tau^+\tau^- q\bar{q}$ in the minimal mixing scenario.

4. Results

No evidence of the production of the h and A bosons is observed in the data. The mass limits are evaluated by calculating the confidence level (CL) that the expected signal is absent in the observed data for the plane defined by $\tan\beta$ and m_h. The CL is calculated using the technique described in Refs. [21,25]. The results of the analyses for all the physics processes and decay channels are combined into bins of one distribution, ordered in the logarithm of signal-over-background. The CL is then calculated from this signal-over-background distribution.

Systematic and statistical errors on the signal and background are considered using the same procedure as in the Standard Model Higgs search [3] taking into account detector uncertainties in the energy scale of the individual sub-detectors, the global energy scale, the tracking and b-tagging efficiencies, and experimental uncertainties in the LEP center-of-mass energy [26] and the luminosity measurement. Theoretical errors on the Higgs boson production cross section due to the uncertainties in α_s [27], interference effects [28] and errors on Higgs decay branching fractions due to quark masses [29] introduce an uncertainty on the predicted number of signal events. The overall systematic error is estimated to be 4% on the number of signal and 10% on the number of background events. The statistical error is larger, but completely uncorrelated among the different bins of the individual channels and is taken into account bin-by-bin [3].

Bins of an analysis with a signal-over-background ratio of less than 0.10 are not considered in the calculation of CL. This cut is chosen to maximize the average CL in the presence of the systematic and statistical error, as calculated from a large set of Monte Carlo experiments. The inclusive signal efficiency for hZ + hA production and the number of selected data and expected background events are shown in Fig. 4a and Fig. 4b for m_h at the average 95% CL limit as a function of $\tan\beta$, before and after the signal-over-background cut. Two examples of the distribution used to calculate the CL are given in Figs. 4c and 4d, for low and high $\tan\beta$ for the m_h point where the CL crosses 95%. No significant excess is observed at any point in the $(m_h, \tan\beta)$ plane for the three mixing scenarios.

Lower limits on the Higgs boson masses as a function of $\tan\beta$ are shown in Fig. 5 for the different mixing hypotheses. The 95% CL lower mass limits on m_A and m_h, as well as the probability to obtain a limit on m_h larger than the one observed, are shown in Table 3 at the two extrema of the scan over $\tan\beta$. In Table 3 we also list the average and median mass limits at the 95% CL, calculated from Monte Carlo, as an indication of the sensitivity of this search. The lowest value of m_h excluded is at $\tan\beta = 20.3$ for typical mixing, and the lowest value of m_A excluded is at $\tan\beta = 22.4$ for minimal mixing. For the MSSM

Table 3

Higgs mass limits in the MSSM from the data at $130\,\text{GeV} \leq \sqrt{s} \leq 183\,\text{GeV}$. At the observed 95% CL, N_{bg}, N_{data} and N_{sig} are respectively the number of events expected from background, the number of observed events and the number of expected signal events from hA + hZ at the $\tan\beta$ listed. The masses $\overline{m}$ and $<m>_{50}$ are respectively the average and median mass limits for the h and A bosons as calculated from a large set of Monte Carlo trials. CL_b is the probability to obtain a mass limit on m_h larger than the one observed. The masses in boldface are the lower mass limits set at the 95% CL from the data

Mixing, $\tan\beta$	N_{events} at 95% CL			Lower mass limits in GeV at 95% CL						
	N_{bg}	N_{data}	N_{sig}	$\overline{m}_h$	$\overline{m}_A$	$<m_h>_{50}$	$<m_A>_{50}$	CL_b	m_h	m_A
minimal, 1				**Excluded to theoretical limit**						
minimal, 50	7.9	7	4.7	69.1	69.1	70.9	70.9	40%	**71.5**	**71.6**
typical, 1	10.3	13	6.1	86.6	187	87.2	212	55%	**87.0**	**209**
typical, 50	6.9	5	4.2	71.2	72.1	72.2	73.1	36%	**72.7**	**73.6**
maximal, 1	10.3	13	6.1	85.6	183	87.2	208	54%	**87.0**	**204**
maximal, 50	7.9	7	4.7	68.9	68.9	70.4	70.5	43%	**71.4**	**71.5**

parameters considered, this results in lower mass limits at the 95% CL of

$$m_h > 70.7 \,\text{GeV}, \quad m_A > 71.0 \,\text{GeV}.$$

Acknowledgements

We acknowledge the efforts of all the engineers and technicians who have participated in the construction and maintenance of L3 and express our gratitude to the CERN accelerator divisions for the superb performance of LEP.

References

[1] S.L. Glashow, Nucl. Phys. 22 (1961) 579; S. Weinberg, Phys. Rev. Lett. 19 (1967) 1264; A. Salam, in Elementary Particle Theory, ed. N. Svartholm, (Almqvist and Wiksell, Stockholm, 1968), p. 367.

[2] P.W. Higgs, Phys. Lett. 12 (1964) 132; F. Englert and R. Brout, Phys. Rev. Lett. 13 (1964) 321; G.S. Guralnik et al., Phys. Rev. Lett. 13 (1964) 585.

[3] L3 Collaboration, M. Acciarri et al., ''Search for the Standard Model Higgs Boson in e^+e^- Interactions at $\sqrt{s} = 183 \,\text{GeV}$'', Preprint EP/98-052, CERN, 1998, Submitted to Phys. Lett. B.

[4] H.P. Nilles, Phys. Rep. 110 (1984) 1; H.E. Haber and G.L. Kane, Phys. Rep. 117 (1985) 75; R. Barbieri, Riv. Nuovo Cim. 11 n°4 (1988) 1.

[5] L3 Collaboration, O. Adriani et al., Phys. Lett. B 294 (1992) 457; O. Adriani et al., Z. Phys. C 57 (1993) 355.

[6] ALEPH Collaboration, D. Buskulic et al., Phys. Lett. B 313 (1993) 312; ALEPH Collaboration, R. Barate et al., Phys. Lett. B 412 (1997) 173; DELPHI Collaboration, P. Abreu et al., Z. Phys. C 67 (1995) 69; DELPHI Collaboration, P. Abreu et al., E. Phys. J. C 2 (1998) 1; OPAL Collaboration, R. Akers et al., Z. Phys. C 64 (1994) 1; OPAL Collaboration, G. Alexander et al., Z. Phys. C 73 (1997) 189; OPAL Collaboration, K. Ackerstaff et al., ''A Search for Neutral Higgs Bosons in the MSSM and Models with Two Scalar Field Doublets'', Preprint EP/98-029, CERN, 1998, Submitted to E. Phys. J. C.

[7] L3 Collaboration, B. Adeva et al., Nucl. Inst. Meth. A 289 (1990) 35; J.A. Bakken et al., Nucl. Inst. Meth. A 275 (1989) 81; O. Adriani et al., Nucl. Inst. Meth. A 302 (1991) 53; B. Adeva et al., Nucl. Inst. Meth. A 323 (1992) 109; K. Deiters et al., Nucl. Inst. Meth. A 323 (1992) 162; M. Chemarin et al., Nucl. Inst. Meth. A 349 (1994) 345; B. Acciari et al.,

Nucl. Inst. Meth. A 351 (1994) 300; G. Basti et al., Nucl. Inst. Meth. A 374 (1996) 293; A. Adam et al., Nucl. Inst. Meth. A 383 (1996) 342.

[8] P. Janot, in Physics at LEP2, ed. G. Altarelli, T. Sjöstrand and F. Zwirner, (CERN 96-01, 1996), volume 2, p. 309.

[9] T. Sjöstrand, ''PYTHIA'', Preprint TH/93-7112, CERN, 1993, revised August 1995; T. Sjöstrand, Comp. Phys. Comm. 82 (1994) 74.

[10] M. Skrzypek et al., Comp. Phys. Comm. 94 (1996) 216; M. Skrzypek et al., Phys. Lett. B 372 (1996) 289.

[11] S. Jadach, B.F.L. Ward and Z. Wąs, Comp. Phys. Comm. 66 (1991) 276.

[12] R. Engel, Z. Phys. C 66 (1995) 203; R. Engel, J. Ranft and S. Roesler, Phys. Rev. D 52 (1995) 1459.

[13] F.A. Berends, R. Pittau and R. Kleiss, Comp. Phys. Comm. 85 (1995) 437.

[14] R. Brun, et al., ''GEANT 3'', Preprint DD/EE/84-1 (Revised), CERN, September 1987.

[15] H. Fesefeldt, RWTH Aachen Preprint PITHA 85/02 (1985).

[16] E. Accomando, in Physics at LEP2, ed. G. Altarelli, T. Sjöstrand and F. Zwirner, (CERN, 1996), volume 1.

[17] R. Barbieri, S. Farrara and C. Savoy, Phys. Lett. B 119 (1982) 343.

[18] CDF Collaboration, F. Abe et al., Phys. Rev. Lett. 74 (1995) 2626; CDF Collaboration, F. Abe et al., ''Measurement of the Top Quark Mass'', Preprint hep-ex/9801014, 1998; D0 Collaboration, S. Abachi et al., Phys. Rev. Lett. 74 (1995) 2632.

[19] M. Biasini et al., ''Standard Model Higgs searches at $\sqrt{s} = 183$ GeV'', L3 Internal Note 2241 (See Section 3.2 for description of cut optimizer), 1998.

[20] L3 Collaboration, M. Acciarri et al., Phys. Lett. B 385 (1996) 454.

[21] L3 Collaboration, M. Acciarri et al., Phys. Lett. B 411 (1997) 373.

[22] S. Bethke et al., Nucl. Phys. B 370 (1992) 310.

[23] J. Branson et al., ''Search for Neutral Higgs Bosons of the Minimal Supersymmetric Standard Model in e^+e^- Interactions at $\sqrt{s} = 130 - 183 \,\text{GeV}$'', L3 Internal Note 2254, 1998.

[24] L3 Collaboration, M. Acciarri et al., Phys. Lett. B 413 (1997) 191.

[25] A. Favara and M. Pieri, ''Confidence Level Estimation and Analysis Optimization'', Preprint DFF-278-4-1997, INFN, 1997.

[26] The Working Group on LEP Energy, ''Preliminary LEP energy calibration for 1997 data'', LEP Energy Group Note 98-01, 1998.

[27] B.A. Kniehl, Phys. Rep. C 240 (1994) 211; E. Gross, B.A. Kniehl and G. Wolf, Z. Phys. C 63 (1994) 417, erratum C 66 (1995) 321.

[28] W. Kilian, M. Krämer and P.M. Zerwas, Phys. Lett. B 373 (1996) 135.

[29] A. Djouadi, M. Spira and P.M. Zerwas, Z. Phys. C 70 (1996) 427.